Multiaxial magnetocrystalline anisotropy in the *X*-type hexaferrite $Sr_2Co_2Fe_{28}O_{46}$ at low temperature

Mai Komabuchi,[1,2] Daisuke Urushihara,[1] Yusuke Kimata,[1] Momoko Okabe,[1] Toru Asaka,[1,2,*] and Koichiro Fukuda[1]

[1]*Divisition of Advanced Ceramics, Nagoya Institute of Technology, Nagoya 466-8555, Japan*

[2]*Frontier Research Institute for Materials Science, Nagoya Institute of Technology, Nagoya 466-8555, Japan*

(Received 8 May 2019; revised manuscript received 5 August 2019; published 4 September 2019)

We investigated the correlation between the crystal structure and magnetism in $Sr_2Co_2Fe_{28}O_{46}$ using magnetic measurements and transmission electron microscopy. With changing temperature, the magnitude of the magnetization along the $[2\bar{1}\bar{1}0]$ and $[01\bar{1}0]$ directions changed drastically at ∼340 K, whereas that along the [0001] direction remained almost unchanged, suggesting a spin reorientation transition. The field dependence of the magnetization along $[2\bar{1}\bar{1}0]$ exhibited characteristic stepwise behavior below 150 K, whereas that along $[01\bar{1}0]$ did not exhibit this behavior, which suggests unusual magnetic anisotropy within the (0001) plane. Evaluation of the magnetic domain structures revealed that $Sr_2Co_2Fe_{28}O_{46}$ exhibits strong axial magnetocrystalline anisotropy with the axis along the direction tilted by ∼60° from the [0001] direction toward the $[01\bar{1}0]$ direction at low temperatures. This anisotropy along a nonunique crystallographic direction results in multiaxial anisotropy because of the crystal symmetry.

DOI: 10.1103/PhysRevB.100.094406

I. INTRODUCTION

Hexaferrites generally have hexagonal or trigonal crystal structures and can be classified into six types (M, W, X, Y, Z, and U) using a combination of three types of structural blocks: R blocks (AFe_6O_{11}), S blocks (spinel, $2MeFe_2O_4$), and T blocks ($A_2Fe_8O_{14}$) [Fig. 1(a)] [1]. Here, *A* denotes typically alkaline-earth ions such as Ba^{2+} and Sr^{2+}, and *Me* denotes divalent metal ions. Hexaferrites have attracted considerable attention because of their various magnetic properties. For instance, M-type hexaferrites, e.g., $BaFe_{12}O_{19}$, exhibit large coercivity and have been applied as permanent magnets [2,3]. In contrast, Y-type and Z-type hexaferrites exhibit soft magnetism with small coercivity and large magnetic permeability [4] and are thus anticipated to be used as high-frequency devices. Recently, some Y-, M-, Z-, and U-type hexaferrites have been reported as multiferroic materials in which ferroelectric and (anti)ferromagnetic order coexist [5–8]. These materials exhibit magnetoelectric effects in which the electric polarization (magnetization) is induced by external magnetic (electric) fields [5–14]. The microscopic mechanisms of these phenomena have been explained using the spin-current model [15], which is also known as the inverse Dzyaloshinskii-Moriya interaction [16].

Magnetic anisotropy means the dependency for magnetic moments in a ferro(ferri)magnet to be directed in one or more directions (generally relative to the crystallographic axes) to decrease the total magnetic energy. There are several types of magnetic anisotropy, including magnetocrystalline and shape anisotropies. Magnetic domain structure is strongly related to such magnetic anisotropies. Strong uniaxial magnetocrystalline anisotropy along the [0001] direction has been observed in M-type barium ferrites using the Bitter technique [2,17]. Similar domain structures have also been observed in barium ferrites using Lorentz electron microscopy [18–21]. In Z-type hexaferrites, magnetic domain structures attributed to the in-plane magnetic anisotropy in the (0001) plane have been observed [22,23].

There are considerably fewer reports on even the fundamental properties of X-type hexaferrites compared with the number of reports on other types of hexaferrites. One of the reasons is the difficulty of synthesizing X-type hexaferrite samples without impurities of M- or W-type hexaferrites [24]. These phases are likely to coexist in the synthesized samples because an X-type hexaferrite $(RSR^*S_2^*)_3$ consists of M-type (RSR^*S^*) and W-type ($RS_2R^*S_2^*$) structural parts, as shown in Fig. 1(b). According to Braun's report on $Ba_2Fe_2^{2+}Fe_{28}^{3+}O_{46}$ ($Me = Fe^{2+}$) [1], the crystal structure of X-type hexaferrites belongs to the trigonal system, and their crystal symmetry is represented by the space group $R\bar{3}m$. The atomic site preferences of Me^{2+} ions have generally been discussed based on structural consideration of W-type hexaferrites [25,26]. The fundamental magnetic properties of X-type hexaferrites have mostly been investigated using polycrystalline samples [24,27–29]. However, to evaluate the intrinsic magnetic properties without effects from the grain size or preferred orientation, single-crystalline samples are required. Using single crystals, Tauber *et al.* [30] reported that $Ba_2Co_2Fe_{28}O_{46}$ has easy-plane anisotropy below 416 K, whereas $Ba_2Zn_2Fe_{28}O_{46}$ exhibits uniaxial anisotropy along [0001] below the Curie temperature. In addition, it has been suggested that $Ba_2Co_2Fe_{28}O_{46}$ has double easy-magnetization cones with a cone axis along the [0001] direction at room temperature [31]. These findings indicate that the magnetocrystalline anisotropy is affected by the species of Me^{2+} ions and the temperature.

*asaka.toru@nitech.ac.jp

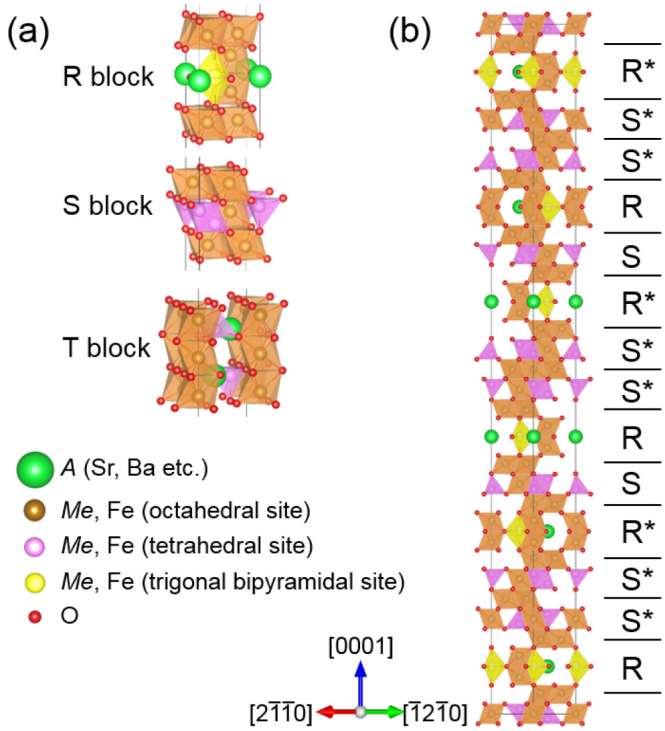

FIG. 1. (a) Structural blocks called R, S, and T blocks. (b) Crystal structure model of an X-type hexaferrite $A_2Me_xFe_{30-x}O_{46}$. The asterisks indicate the structural blocks rotated by 180° around the hexagonal c axis.

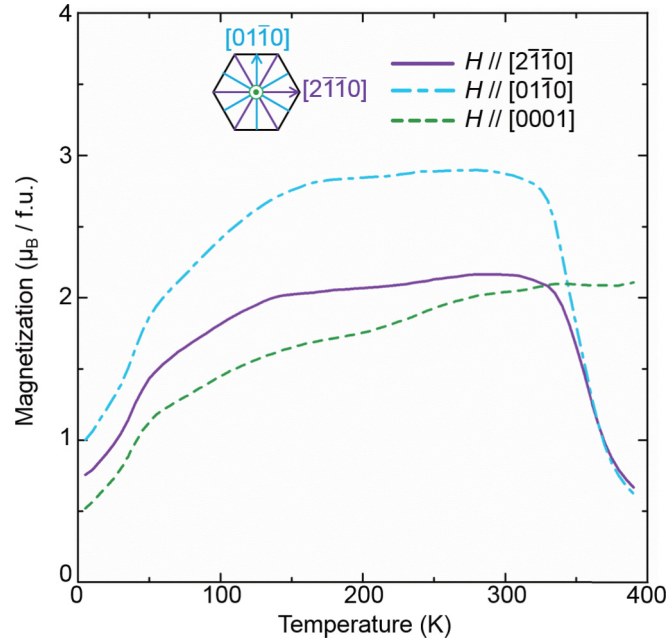

FIG. 2. Temperature dependence of magnetization upon heating after ZFC. The magnetic fields (H = 100 Oe) were applied parallel to the [2$\bar{1}\bar{1}$0], [01$\bar{1}$0], and [0001] directions.

In this study, we observed peculiar magnetocrystalline anisotropy in a single crystal of the X-type hexaferrite $Sr_2Co_2Fe_{28}O_{46}$. We evaluated the magnetic domain structures of $Sr_2Co_2Fe_{28}O_{46}$ using Lorentz transmission electron microscopy (LTEM) to explain the magnetocrystalline anisotropy, and we discuss the origin of the magnetocrystalline anisotropy from the atomistic viewpoint.

II. EXPERIMENTS

Single crystals of $Sr_2Co_2Fe_{28}O_{46}$ were prepared using a flux method. $SrCO_3$, Co_3O_4, Fe_2O_3, and Na_2CO_3 were mixed at a molar ratio of 13.2 : 2.5 : 67.8 : 16.5. The mixtures were packed into a platinum crucible and then heated at 50 K/h and held at 1620 K for 48 h in a tube furnace. The mixtures were then cooled to 1480 K at 0.5 K/h and then to room temperature at 150 K/h. These procedures were conducted in O_2 flow. The single crystals were obtained by dissolving the flux in nitric acid. The typical size of the obtained hexagonal-plate-like crystals was a length of 3–5 mm and a thickness of 1 mm.

The crystal phase of each of the obtained crystals was identified using Co-$K\alpha$ radiation (MiniFlex600, Rigaku). To estimate the crystal orientation, a Laue camera with an imaging plate (IPX-LC, IPX) was used. We used the Fresnel method of LTEM for imaging the domain structures, and the local magnetization was calculated using the software QPT for DigitalMicrograph [32] based on the transport-of-intensity equation (TIE) method [33,34]. Annular dark-field (ADF) images were obtained using scanning transmission electron microscopy (STEM), and atomic-resolution energy-dispersive x-ray spectroscopy (EDS) analysis was also performed. A JEM-ARM200F transmission electron microscope (JEOL) operated at 200 kV was used. The single crystal was cut into approximately 1 mm × 1 mm × 1 mm for magnetic measurements. The magnetization was measured using a superconductive quantum interference device magnetometer (MPMS, Quantum Design). The magnetic fields were applied along the [2$\bar{1}\bar{1}$0], [01$\bar{1}$0], and [0001] directions.

III. RESULTS AND DISCUSSION

Figure 2 shows the temperature dependence of the magnetization upon heating after zero-field cooling (ZFC). Magnetic fields of 100 Oe were applied along the [2$\bar{1}\bar{1}$0], [01$\bar{1}$0], and [0001] directions. Above 340 K, the easy direction of the magnetization was assumed to be the [0001] direction, which indicates that the sample exhibited uniaxial magnetic anisotropy in the [0001] direction. The magnetization parallel to the [2$\bar{1}\bar{1}$0] and [01$\bar{1}$0] directions drastically changed at 340 K, whereas the [0001] magnetization remained almost unchanged. Below this temperature, the magnetization parallel to the [01$\bar{1}$0] direction was the largest of those in the three directions. The easier magnetization direction appeared to be the [01$\bar{1}$0] direction rather than the [0001] direction. The slopes of the graphs clearly changed at approximately 50 and 150 K, indicating that certain magnetic changes occurred at each temperature.

When the magnetic fields H were swept along the [2$\bar{1}\bar{1}$0] direction at low temperature, the magnetization M changed stepwise at external magnetic fields of approximately 0.3 and 1.5 T [Fig. 3(a)]. The magnetic fields required for saturating magnetization decreased with increasing temperature,

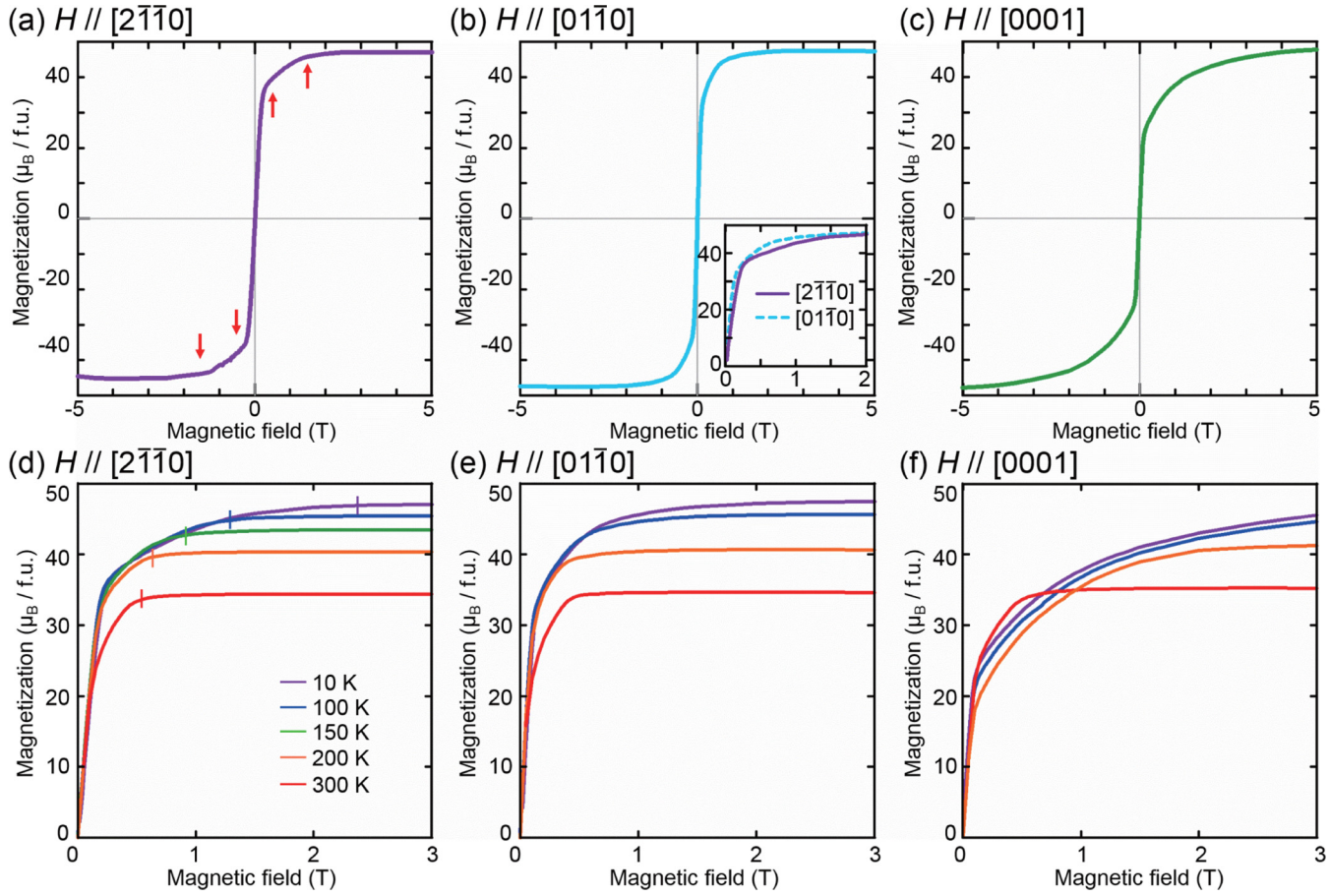

FIG. 3. Magnetic field dependence of magnetization measured at 10 K when the external magnetic fields were applied along the (a) [2$\bar{1}\bar{1}$0], (b) [01$\bar{1}$0], and (c) [0001] directions. The magnetization curve in (a) changed stepwise at the points indicated by the red arrows. The differences in the behavior between [2$\bar{1}\bar{1}$0] and [01$\bar{1}$0] at 10 K are shown in the inset of (b). (d)–(f) Magnetization curves at various temperatures between 10 and 300 K. The vertical lines in (d) indicate the saturation points of magnetization at the respective temperatures.

and the stepwise changes disappeared above 150 K [Fig. 3(d)]. In contrast, this behavior was not observed in the [01$\bar{1}$0] direction at any temperature [Figs. 3(b) and 3(e)]. The magnetization along the [01$\bar{1}$0] direction saturated at lower magnetic fields than the case of $H \parallel [2\bar{1}\bar{1}0]$. These results indicate that $Sr_2Co_2Fe_{28}O_{46}$ exhibits strong magnetocrystalline anisotropy in the (0001) plane below 150 K. To the best of our knowledge, such magnetic anisotropy has not been reported for other hexaferrites. The stepwise changes were not observed in the [2$\bar{1}\bar{1}$0] nor [01$\bar{1}$0] directions above 200 K, which indicates that the magnetocrystalline anisotropy between these two directions became weaker during heating up to 200 K. Below room temperature, the external magnetic field needed to saturate the magnetization for the [0001] direction was the largest among those in the three directions [Fig. 3(c)]. However, the magnetic anisotropy in the three directions appeared to be weak near room temperature [Figs. 3(d)–3(f)].

Figures 4(a)–4(c) present the Fresnel images for the (2$\bar{1}\bar{1}$0) plane, taken with the incident beam parallel to the [2$\bar{1}\bar{1}$0] direction at 103, 295, and 393 K, respectively, and the calculated local magnetizations for the respective images are presented in Figs. 4(d)–4(f). The bright and dark straight lines in the Fresnel images correspond to magnetic domain walls. The 180° magnetic domain structures were formed at every temperature in this plate [Figs. 4(a) and 4(d)]. The magnetic moments in these domains were not along the [01$\bar{1}$0] or [0001] direction at 103 K. Upon heating to room temperature, partial closure domains were formed [Figs. 4(b) and 4(e)], which suggests that the uniaxial magnetic anisotropy in this plane became weaker. Moreover, the 180° domain walls along the [0001] direction were formed above ∼340 K [Figs. 4(c) and 4(f)]. This domain structure clearly indicates uniaxial magnetocrystalline anisotropy with an easy axis parallel to the [0001] direction. This finding is consistent with the magnetic measurements indicating that the spin reorientation transition occurred at ∼340 K. The spin reorientation behavior is quite a contrast to that of another X-type hexaferrite $Sr_2Fe_2^{2+}Fe_{28}^{3+}O_{46}$ ($Me^{2+} = Fe^{2+}$), in which temperature-independent magnetocrystalline anisotropy has been observed [35]. This suggests that Co^{2+} ion significantly affects the magnetocrystalline anisotropy in X-type hexaferrites.

The directions of the local magnetization around a domain wall at 103 K are shown in Figs. 5(a) and 5(b) as a vector map and heat map, respectively. Antiparallel magnetic moments existed overall and were oriented in the direction tilted by

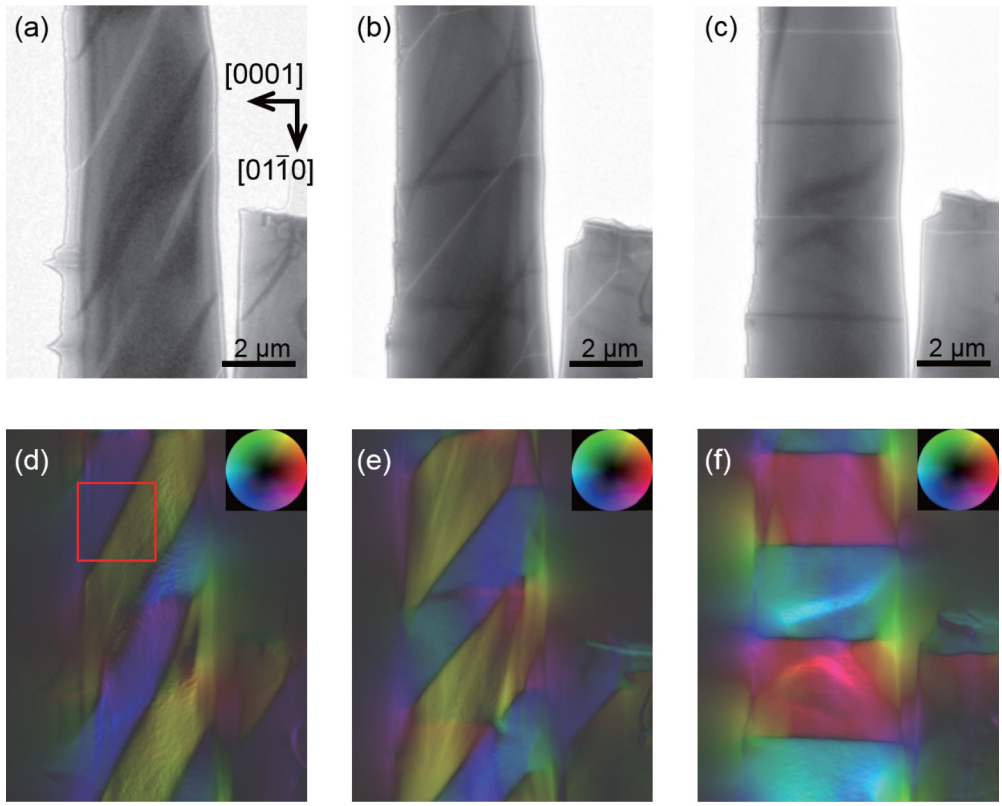

FIG. 4. LTEM images of the (2$\bar{1}\bar{1}$0) plane taken at (a) 103 K, (b) 295 K, and (c) 393 K with defocus values of 1.8, 0.6, and 0.6 mm, respectively. (d), (e), and (f) Magnetization distribution maps for (a), (b), and (c), respectively, calculated using the TIE method. The magnitude and directions of the local magnetic moments are indicated by the brightness and color phase, referring to the color wheel.

$\sim$60° from the [0001] direction toward the [01$\bar{1}$0] direction. This magnetic domain structure indicates that the sample exhibited strong uniaxial magnetocrystalline anisotropy in the (2$\bar{1}\bar{1}$0) plane and that the easy direction was not along the low-index crystallographic axes in the trigonal structure at low temperatures. From the electron diffraction pattern from this area [Fig. 5(c)], the crystal orientation in this plane can be identified as shown in Fig. 5(d). Most of the magnetic moments pointed in the direction from the center transition metal atom to the oxygen atoms at the vertices of the (Fe, *Me*)O_6 octahedra in S*S* blocks, i.e., the direction along the dashed line in Fig. 5(d).

Figure 6(a) presents an ADF-STEM image taken with the incident beam parallel to the [2$\bar{1}\bar{1}$0] direction, and Figs. 6(b)–6(d) present the EDS maps obtained using Sr-*L*, Fe-*K*, and Co-*K* signals in the same area and are overlaid in Fig. 6(e). The intensity of ADF-STEM images depends on the atomic number *Z*, and atomic columns can appear as bright spots. The Co-*K* signals were strongly detected at the center of S*S* blocks, which indicates that the Co^{2+} ions were localized at the octahedral sites in S* blocks. The site preference of Co^{2+} ions in S blocks has been reported in W-type hexaferrites including Co^{2+} investigated using neutron diffraction [25] and nuclear magnetic resonance [26]. For X-type hexaferrites, a similar preference has also been suggested based on the magnitudes of their spontaneous magnetizations [24,29,30]. In the current work, we succeeded in directly observing the preference of Co^{2+} for these specific sites using STEM-EDS.

The aforementioned Co^{2+} site in the S* block is identical to the octahedral site in spinel ferrites. In the Co-substituted magnetite $Co_xFe_{3-x}O_4$ and cobalt ferrite $CoFe_2O_4$ with inverse spinel structure, Co^{2+} mostly occupies the octahedral sites. In such spinel ferrites, Co^{2+} ions principally contribute to the spontaneous magnetization in the ferrimagnetism because the antiparallel couples of the spin moments on Fe^{3+} ions cancel each other [2]. In addition, the spinel ferrites have easy axes of magnetization of ⟨100⟩ in the cubic lattice [36], resulting from a one-ion model at Co^{2+} sites [37–40]. Here, ⟨100⟩ is parallel to the direction of the vertex oxygen from Co^{2+} (Fe^{3+}) at the octahedra. Based on these properties in spinel ferrites, it is reasonable to conclude that Co^{2+} ions at the octahedral site in S* block induce the uniaxial magnetocrystalline anisotropy to the vertex directions of the (Fe, *Me*)O_6 octahedra at low temperatures in $Sr_2Co_2Fe_{28}O_{46}$. Although the one-ion anisotropy can be evaluated from magnetic anisotropy constants [41], those constants of the present compound calculated by phenomenological analysis [42–44] were incompatible with the results of LTEM observation. This calculation failure would be caused by the below-mentioned extraordinary magnetic anisotropy.

In the (01$\bar{1}$0) plane, fine stripe subdomains appeared in the primary domains at 84 K [Fig. 7(a)]. Note that the straight lines perpendicular to the [0001] direction are cleavages

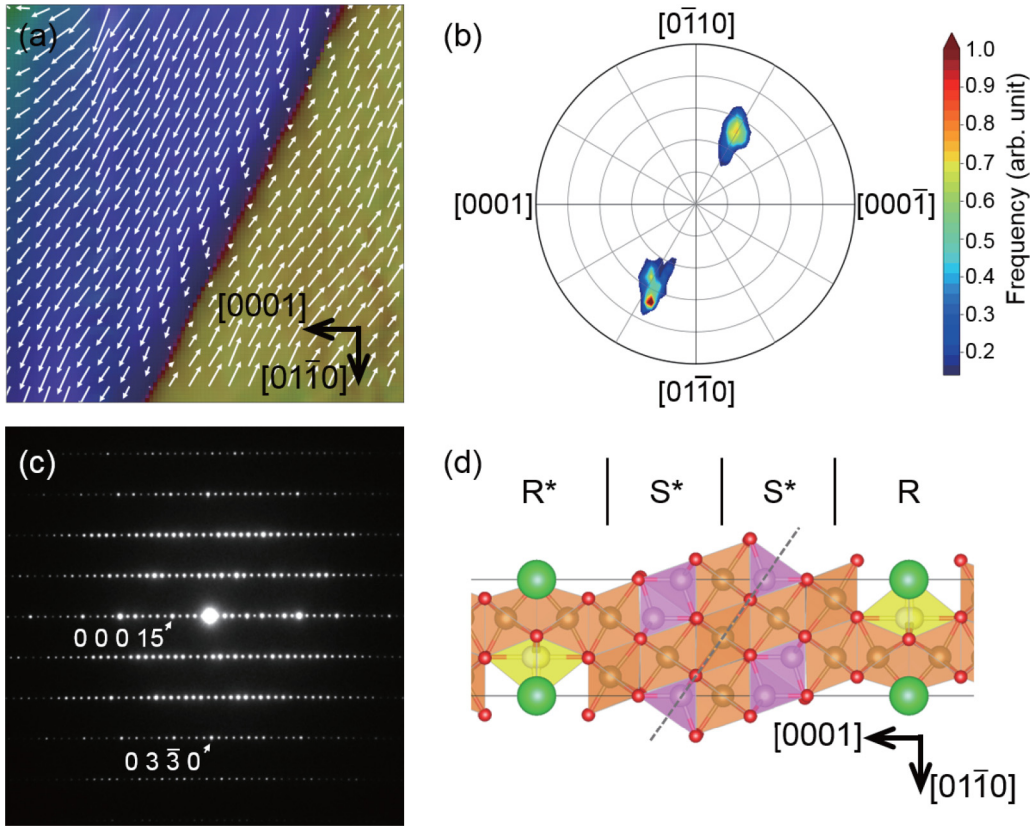

FIG. 5. (a) Enlarged image of the region surrounded by the red square in Fig. 4(d). The white arrows represent the directions and magnitude of the local magnetization at each point. (b) Tendency of local magnetization in (a) as normalized frequency distribution. (c) Electron diffraction pattern of observed area. (d) Crystal structure around the S*S* blocks corresponding to the crystal orientation shown in (c). The dashed line denotes one of the body-diagonal directions of the (Fe, *Me*)O_6 octahedron in the S* blocks. This line is almost along the magnetization direction.

of the specimen. The subdomain walls were roughly along the [0001] direction, and the typical subdomain width was ~200 nm, which is completely different from the observations of the (2$\bar{1}\bar{1}$0) plane [Fig. 4(a)]. Thus, the strong magnetic anisotropy within the (0001) plane was also confirmed by the magnetic domain observation. Such stripe patterns are often observed in samples with uniaxial anisotropy out of the observing plane [45,46]. In thin-plate specimens for transmission electron microscopy observation, magnetic moments usually lie on the plate to reduce the magnetostatic energy. However, for strong magnetocrystalline anisotropy out of a thin plane, magnetic moments are inclined from the plane. Consequently, narrow stripe domains with directional alternation of local magnetization are formed to minimize the total magnetic energy. Thus, these experiments clearly demonstrate that $Sr_2Co_2Fe_{28}O_{46}$ exhibits strong magnetocrystalline anisotropy out of the (01$\bar{1}$0) plane below 150 K. The subdomain walls in Fig. 7(a) were almost along the [0001]

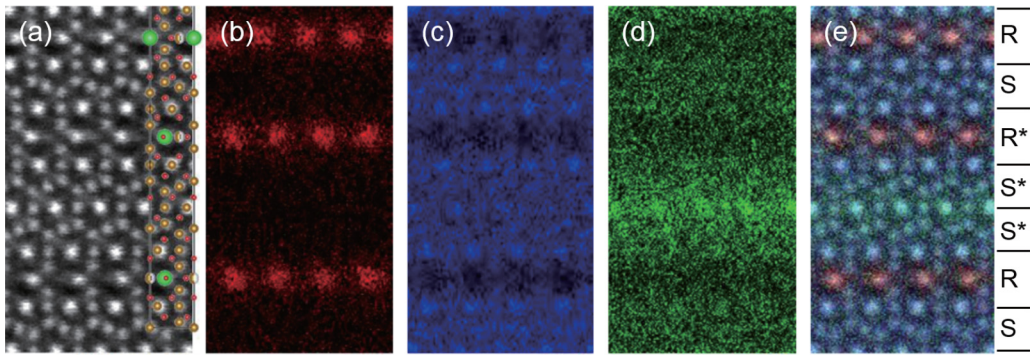

FIG. 6. (a) ADF-STEM image taken with the incident beam parallel to the [2$\bar{1}\bar{1}$0] direction. The inset shows the crystal structure of the X-type hexaferrite. The color maps indicate the positions at which (b) Sr-*L*, (c) Fe-*K*, and (d) Co-*K* signals were detected by EDS. (a)–(d) are overlaid in (e).

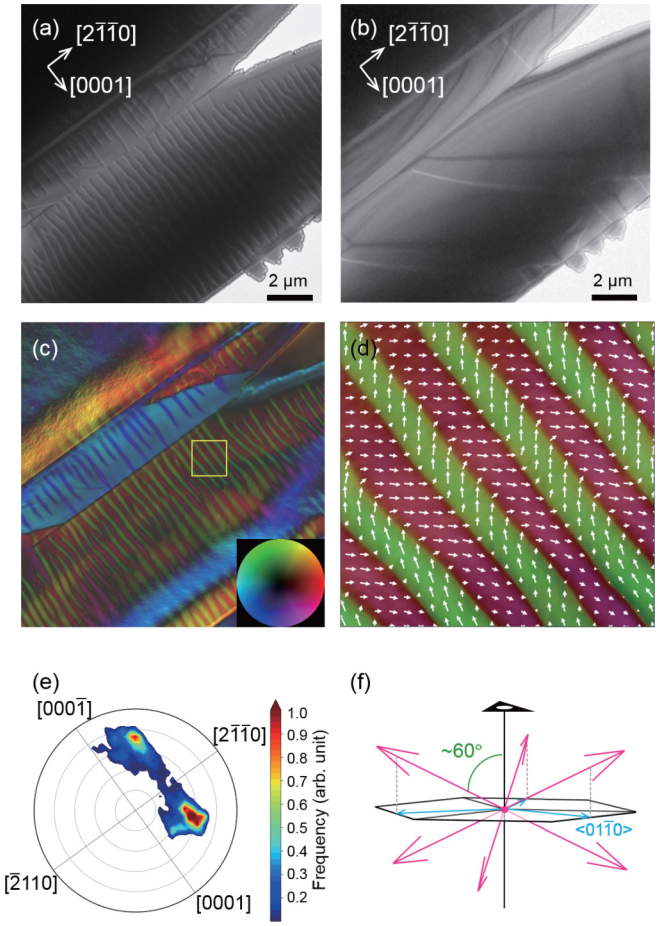

FIG. 7. LTEM images of the (01$\bar{1}$0) plane taken at (a) 84 K and (b) 295 K with a defocus value of 0.9 mm. (c) Magnetization-distribution map of (a), referring to the color wheel shown in the inset, calculated using the TIE method. (d) Enlarged image of the region surrounded by the yellow square in (c). The white arrows represent the directions and magnitude of the local magnetization at each location. (e) Tendency of the local magnetization in (d) as normalized frequency distribution. (f) Schematic illustration of the easy directions below 150 K based on the threefold rotoinversion axis along the *c* axis.

direction. However, the local magnetic moments were not along their domain walls and fluctuated periodically [Figs. 7(c)–7(e)]. Based on the threefold rotoinversion axis along the *c* axis, three equivalent easy axes should exist, as shown in Fig. 7(f). This magnetic anisotropy is distinctly different from the so-called "easy-cone" anisotropy and more similar to the three-canted uniaxial one, i.e., multiaxial anisotropy. Note that TIE calculation gives the magnetization components within the observing plane. In one of the major magnetic domains, the competition of the two easy axes near the observing plane dominantly caused the zigzag distribution of magnetization between subdomains [Fig. 7(d)]. The magnetic domains would have been rearranged to minimize the total of the magnetocrystalline and magnetostatic energies. Near room temperature, ordinary closure domains were formed instead of the stripe domains [Fig. 7(b)], and the strong magnetocrystalline anisotropy out of the (01$\bar{1}$0) plane was no longer observed. Combined with the domain structure of the (2$\bar{1}\bar{1}$0) plane, the ferromagnetism at ∼150 to ∼340 K appears to have an easy-cone anisotropy. The axis of the easy cone is parallel to [0001], and its half apex angle is estimated at ∼50° around 300 K.

Stepwise behavior has been observed in the magnetization curves of Y- and Z-type hexaferrites with a helical magnetic structure [5,47] and conical magnetic structure [11,12,48,49], respectively. The magnetic anisotropy between [2$\bar{1}\bar{1}$0] and [01$\bar{1}$0], however, cannot be explained with helical or conical magnetic structures. In addition, the present compound does not exhibit lattice modulations accompanied with the helical magnetic structure, as observed in Y-type hexaferrite [50]. Moreover, the characteristic magnetic domain structures observed in the conical magnet, Z-type hexaferrite [23] were not observed in the current Fresnel images. Even though the helical or conical magnetic structures cannot be ruled out until detailed measurements are performed using another technique such as neutron diffraction, the differences between [2$\bar{1}\bar{1}$0] and [01$\bar{1}$0] in the magnetization curves below 150 K can be explained by consideration of the multiaxial magnetocrystalline anisotropy. In both cases of the magnetic fields parallel to the [2$\bar{1}\bar{1}$0] and [01$\bar{1}$0] directions, the magnetic domains are developed along the direction of the magnetic fields during the initial magnetization process. After the unification of magnetic domains, the magnetic moments begin to rotate toward the direction of the magnetic fields. This rotation mechanism of magnetic moments differs depending on the magnetic field direction. When the magnetic fields are applied parallel to the [2$\bar{1}\bar{1}$0] direction, the magnetic moments first turn to the direction of an easy axis on the (01$\bar{1}$0) plane. Next, the magnetic moments are oriented to the [2$\bar{1}\bar{1}$0] direction. Magnetic domain models and the behavior of magnetic moments are shown in Fig. 8(a). These two-step rotations cause the stepwise changes in the magnetization curve. However, for the [01$\bar{1}$0] direction, the magnetic moments along an easy axis rotate to the [01$\bar{1}$0] direction immediately after magnetic domain unification [Fig. 8(b)]. Therefore, the behavior of the magnetization curve is similar to that of ordinary ferromagnetic substances.

IV. CONCLUSIONS

We evaluated the magnetocrystalline anisotropy of an X-type hexaferrite $Sr_2Co_2Fe_{28}O_{46}$. The present compound exhibits various magnetocrystalline anisotropies via the spin-reorientation transitions; the uniaxial magnetocrystalline anisotropy above ∼340 K, the cone one between ∼150 and ∼340 K, and the canted uniaxial one below ∼150 K. The canted uniaxial magnetocrystalline anisotropy state leads to the three easy axes along the directions tilted by ∼60° from the [0001] direction toward each ⟨01$\bar{1}$0⟩ one from the crystal symmetry, i.e., multiaxial magnetocrystalline anisotropy. It is possible that the origin of this peculiar magnetocrystalline anisotropy is the Co^{2+} ions localized at the (Fe, *Me*)O_6 octahedral site in the couples of the S* blocks. The stepwise changes in the magnetization curves ($H \parallel$ [2$\bar{1}\bar{1}$0]) were caused by the multistep magnetization process during which the magnetic domain unification and rotation of the magnetic moments occurred.

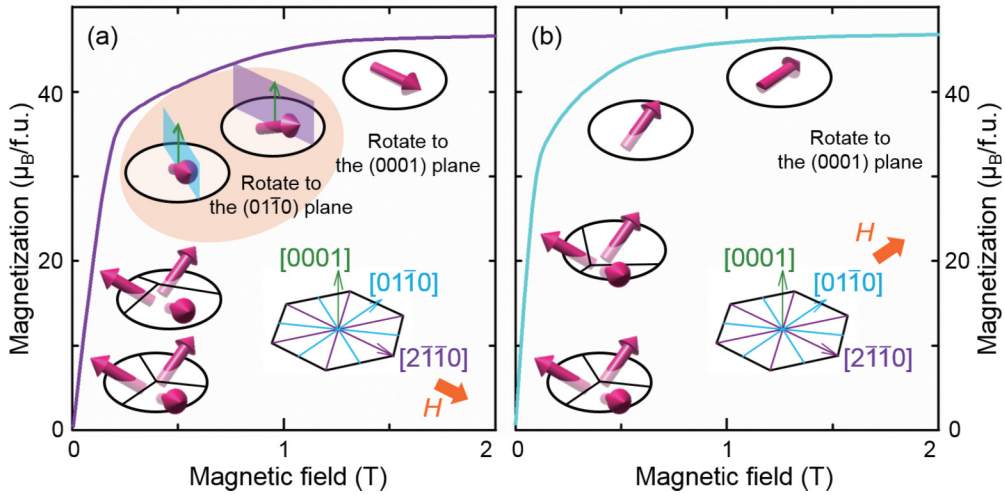

FIG. 8. Schematic illustrations of the magnetic moments and domains in the saturation process of magnetization below 150 K. The magnetic fields were applied along the (a) [2$\bar{1}\bar{1}$0] and (b) [01$\bar{1}$0] directions. The arrows in the respective circles indicate the directions of the magnetic moments.

ACKNOWLEDGMENTS

We thank T. Kimura, K. Kimura, S. Hirose, H. Kawase, M. Konoto, and K. Yamamoto for their fruitful discussions. We are grateful to H. Ueda for his valuable suggestions. This work was partly supported by Nanotechnology Platform Program (Molecule and Material Synthesis) of the Ministry of Education, Culture, Sports, Science and Technology (MEXT), Japan.

[1] P. B. Braun, Philips Res. Rep. **12**, 491 (1957).
[2] J. Smit and H. P. J. Wijn, Ferrites (Philips Technical Library, Eindhoven, 1959).
[3] V. V. Pankov, M. Pernet, P. Germi, and P. J. Mollard, Magn. Magn. Mater. **120**, 69 (1993).
[4] A. L. Stuijts and H. P. J. Wijn, J. Appl. Phys **29**, 468 (1958).
[5] T. Kimura, G. Lawes, and A. P. Ramirez, Phys. Rev. Lett. **94**, 137201 (2005).
[6] Y. Tokunaga, Y. Kaneko, D. Okuyama, S. Ishiwata, T. Arima, S. Wakimoto, K. Kakurai, Y. Taguchi, and Y. Tokura, Phys. Rev. Lett. **105**, 257201 (2010).
[7] Y. Kitagawa, Y. Hiraoka, T. Honda, T. Ishikura, H. Nakamura, and T. Kimura, Nat. Mater. **9**, 797 (2010).
[8] K. Okumura, T. Ishikura, M. Soda, T. Asaka, H. Nakamura, Y. Wakabayashi, and T. Kimura, Appl. Phys. Lett. **98**, 212504 (2011).
[9] S. Shen, Y. Chai, and Y. Sun, Sci. Rep. **5**, 8254 (2015).
[10] K. Okumura, K. Haruki, T. Ishikura, S. Hirose, and T. Kimura, Appl. Phys. Lett. **103**, 032906 (2013).
[11] S. H. Chun, Y. S. Chai, B.-G. Jeon, H. J. Kim, Y. S. Oh, I. Kim, H. Kim, B. J. Jeon, S. Y. Haam, J.-Y. Park, S. H. Lee, J.-H. Chung, J.-H. Park, and K. H. Kim, Phys. Rev. Lett. **108**, 177201 (2012).
[12] S. Hirose, K. Haruki, A. Ando, and T. Kimura, Appl. Phys. Lett. **104**, 022907 (2014).
[13] V. Kocsis, T. Nakajima, M. Matsuda, A. Kikkawa, Y. Kaneko, J. Takashima, K. Kakurai, T. Arima, F. Kagawa, Y. Tokunaga, Y. Tokura, and Y. Taguchi, Nat. Commun. **10**, 1247 (2019).
[14] K. Taniguchi, N. Abe, S. Ohtani, H. Umetsu, and T. Arima, Appl. Phys. Express **1**, 031301 (2008).
[15] H. Katsura, N. Nagaosa, and A. V. Balatsky, Phys. Rev. Lett. **95**, 057205 (2005).
[16] I. A. Sergienko and E. Dagotto, Phys. Rev. B **73**, 094434 (2006).
[17] R. Gemperle, V. Kamberský, J. Šimšová, L. Murtinová, L. Půst, P. Görnet, W. Schüppel, and R. Gerber, J. Magn. Magn. Mater. **118**, 295 (1993).
[18] P. J. Grundy, Br. J. Appl. Phys. **16**, 409 (1965).
[19] X. Z. Yu, M. Mostovoy, Y. Tokunaga, W. Zhang, K. Kimoto, Y. Matsui, Y. Kaneko, N. Nagaosa, and Y. Tokura, Proc. Natl. Acad. Sci. USA **109**, 8856 (2012).
[20] X. Z. Yu, K. Shibata, W. Koshibae, Y. Tokunaga, Y. Kaneko, T. Nagai, K. Kimoto, Y. Taguchi, N. Nagaosa, and Y. Tokura, Phys. Rev. B **93**, 134417 (2016).
[21] H. Nakajima, A. Kotani, K. Harada, Y. Ishii, and S. Mori, Phys. Rev. B **94**, 224427 (2016).
[22] G. A. Jones, M. Toy, J. G. Booth, and C. E. Turner, J. Magn. Magn. Mater. **131**, 29 (1994).
[23] H. Nakajima, H. Kawase, K. Kurushima, A. Kotani, T. Kimura, and S. Mori, Phys. Rev. B **96**, 024431 (2017).
[24] K. Kamishima, N. Hosaka, K. Kakizaki, and N. Hiratsuka, J. Appl. Phys. **109**, 013904 (2011).
[25] A. Collomb, B. Lambert-Anderson, J. X. Boucherle, and D. Samaras, Phys. Status Solidi A **96**, 385 (1986).
[26] G. Albanese, E. Calabrese, A. Deriu, and F. Licci, Hyperfine Interact. **28**, 487 (1986).
[27] S. Dey and R. Valenzuela, J. Appl. Phys. **55**, 2340 (1984).
[28] F. Leccabue, G. Albanese, and O. A. Muzio, J. Appl. Phys. **61**, 2600 (1987).
[29] B. X. Gu, J. Appl. Phys. **71**, 5103 (1992).
[30] A. Tauber, J. S. Megill, and J. R. Shappirio, J. Appl. Phys. **41**, 1353 (1970).

[31] G. A. Jones, S. F. H. Parker, J. G. Booth, and D. Simkin, IEEE Trans. Magn. **26**, 2084 (1990).
[32] K. Ishizuka and B. Allman, J. Electron Microsc. **54**, 191 (2005).
[33] M. Teague, J. Opt. Soc. Am. **73**, 1434 (1983).
[34] D. Paganin and K. A. Nugent, Phys. Rev. Lett. **80**, 2586 (1998).
[35] H. Ueda, H. Shakudo, H. Santo, Y. Fujii, C. Michioka, and K. Yoshimura, J. Phys. Soc. Jpn. **87**, 104706 (2018).
[36] R. M. Bozorth, E. F. Tilden, and A. J. Williams, Phys. Rev. **99**, 1788 (1955).
[37] J. C. Slonczewski, J. Appl. Phys. **32**, S253 (1961).
[38] J. C. Slonczewski, J. Appl. Phys. **29**, 448 (1958).
[39] J. C. Slonczewski, Phys. Rev. **110**, 1341 (1958).
[40] M. Tachiki, Prog. Theor. Phys. **23**, 1055 (1960).
[41] D. Alders, R. Coehoorn, and W. J. M. de Jonge, Phys. Rev. B **63**, 054407 (2001).
[42] W. Sucksmith and J. E. Thompson, Proc. R. Soc. London, Ser. A **225**, 362 (1954).
[43] H. Ueda, Y. Tanioku, C. Michioka, and K. Yoshimura, Phys. Rev. B **95**, 224421 (2017).
[44] D. Samaras, A. Collomb, S. Hadjivasiliou, C. Achilleos, J. Tsoukalas, J. Pannetier, and J. Rodrigues, J. Magn. Magn. Mater. **79**, 193 (1989).
[45] N. Saito, H. Fujiwara, and Y. Sugita, J. Phys. Soc. Jpn. **19**, 421 (1964).
[46] V. R. Matricardi, W. G. Lehmann, N. Kitamura, and J. Silcox, J. Appl. Phys. **38**, 1297 (1967).
[47] N. Momozawa, Y. Yamaguchi, H. Takei, and M. Mita, J. Phys. Soc. Jpn. **54**, 771 (1985).
[48] S. Ishiwata, Y. Taguchi, H. Murakawa, Y. Onose, and Y. Tokura, Science **319**, 1643 (2008).
[49] M. Soda, T. Ishikura, H. Nakamura, Y. Wakabayashi, and T. Kimura, Phys. Rev. Lett. **106**, 087201 (2011).
[50] T. Asaka, X. Z. Yu, Y. Hiraoka, K. Kimoto, T. Hirayama, T. Kimura, and Y. Matsui, Phys. Rev. B **83**, 130401(R) (2011).